A calibration of the relation between the abundance of close galaxy pairs and the rate of galaxy mergers

M. G. Kitzbichler⋆ and S. D. M. White
Max-Planck Institut für Astrophysik, Karl-Schwarzschild-Straße 1, D-85748 Garching b. München, Germany

11 April 2008

ABSTRACT
Estimates of galaxy merger rates based on counts of close pairs typically assume that most of the observed systems will merge within a few hundred Myr (for projected pair separations $\leqslant 25h^{-1}$ kpc). Here we investigate these assumptions using virtual galaxy catalogues derived from the Millennium Simulation, a very large N-body simulation of structure formation in the concordance ΛCDM cosmology. These catalogues have been shown to be at least roughly consistent with a wide range of properties of the observed galaxy population at both low and high redshift. Here we show that they also predict close pair abundances at low redshift which agree with those observed. They thus embed a realistic and realistically evolving galaxy population within the standard structure formation paradigm, and so are well-suited to calibrate the relation between close galaxy pairs and mergers. We show that observational methods, when applied to our mock galaxy surveys, do indeed identify pairs which are physically close and due to merge. The sample-averaged merging time depends only weakly on the stellar mass and redshift of the pair. At $z \leqslant 2$ this time-scale is $T \approx T_o r_{25} M_*^{-0.3}$, where r_{25} is the maximum projected separation of the pair sample in units of $25h^{-1}$kpc, M_* is the typical stellar mass of the pairs in units of $3 \times 10^{10}h^{-1}M_\odot$, and the coefficient T_0 is 1.1 Gyr for samples selected to have line-of-sight velocity difference smaller than 300 km/s and 1.6 Gyr for samples where this velocity difference is effectively unconstrained. These timescales increase slightly with redshift and are longer than assumed in most observational studies, implying that merger rates have typically been overestimated.

Key words: galaxies: general – galaxies: formation – galaxies: evolution – galaxies: interactions – galaxies: statistics

1 INTRODUCTION

Ever since the pioneering work of Holmberg (1937) the study of close pairs has been considered an important tool for understanding galaxies. Early work was primarily directed towards comparing properties such as luminosity, colour, and morphology with those of isolated systems, but also recognised that the dynamics of close pairs can be used to estimate their masses (e.g. Page 1952). Close pairs seemed a natural key to understanding the initially speculative idea that galaxies might frequently merge. This was first championed by Toomre & Toomre (1972) in their famous study of the dynamics of interacting spiral galaxies, and as it was gradually accepted, mergers came to be seen as an important factor shaping the observed galaxy population, in particular, producing elliptical galaxies (e.g. Fall 1979). In its Cold Dark Matter (CDM) incarnation, the hierarchical picture of structure growth gained ascendancy throughout the 1980's and 1990's, and with it came ever more detailed models which integrated merging into the build-up both of

the stellar masses and of the morphological properties of galaxies (e.g. Kauffmann, White, & Guiderdoni 1993). Observational estimates of galaxy merger rates thus became a critical test of the ideas underlying these theoretical models.

A number of studies have used close pair counts to estimate merger rates as a function of redshift (Zepf & Koo 1989; Burkey et al. 1994; Woods et al. 1995; Patton et al. 1997; Le Fèvre et al. 2000). Such studies assume that the observed pairs will merge on a rather short timescale, provided they satisfy certain conditions that indicate that they are on a tightly bound orbit. The inferred merger rate is inversely proportional to the adopted timescale, so the results of such studies depend critically on choosing the correct timescale with the correct dependence on pair properties and on redshift. Studies using this method have yielded a wide variety of results, a diversity which can be attributed to differences in pair definition and in the timescales adopted. No consistent picture has so far emerged.

A different technique which has become popular more recently is the identification of mergers *a posteriori* through the disturbed morphology of the merger remnants. An apparent advantage

⋆ E-mail: mgk@mpa-garching.mpg.de

is that one doesn't have to make any assumption about whether and when a merger will occur. Instead the merger can be taken as a fact. On the other hand, one must adopt a timescale over which the disturbed morphology remains visible, and this timescale is likely to depend on redshift, on observing conditions, and on the detailed properties of the merging systems. In practice it is highly uncertain. In addition, this method requires high-resolution, high signal-to-noise imaging, and has therefore become possible for the distant universe only in the last decade with the advent of efficient space-borne imagers.

The most recent attempts to estimate merger rates with each of these methods (Lin et al. 2004; Lotz et al. 2006; Bell et al. 2006) have indicated that evolution with redshift is much weaker than found in earlier observational analyses and inferred from theoretical treatments of the merging of dark-matter halos (e.g. Lacey & Cole 1993; Khochfar & Burkert 2001). Berrier et al. (2006) gave an possible explanation for this discrepancy based on halo-occupation-distribution (HOD) modelling of galaxy clustering. They concluded that the galaxy merger rate does not mirror the halo merger rate because it is strongly affected by the additional processes which govern the merging of galaxies within a common halo. This was demonstrated explicitly by Guo & White (2008) using the Millennium Simulation galaxy catalogues we analyse below. They found that whereas specific merger rates for dark halos depend weakly on mass and strongly on redshift, the opposite is true for galaxies, at least for the particular galaxy formation model they analysed.

In the current paper, our focus is not on understanding these theoretical issues, but rather on checking the assumptions which are made when estimating galaxy merger rates from counts of close pairs. In particular, we calibrate the relevant timescales as a function of pair properties and of redshift. We identify close pairs in virtual galaxy catalogues following standard observatonal criteria, and we study whether and when these pairs merge. The simulated galaxies are embedded in a dynamically consistent way within a realisation of the concordance ΛCDM cosmology. Furthermore, their properties and their small-scale clustering are a reasonably good match to observation. Thus, we believe that the relation between close pairs and mergers in the simulation should be similar to that in the real universe.

Our paper is organised as follows. In Section 2 we summarise the properties of the Millennium Simulation (Springel et al. 2005) and the associated galaxy catalogues that we analyse here. The latter are based on the fiducial model of Croton et al. (2006) as modified by De Lucia & Blaizot (2007) and extended by Kitzbichler & White (2007). We describe the treatment of galaxy mergers in this model and the connection between close galaxy pairs and mergers. We also contrast the behaviour of galaxy and halo merger rates. Section 3 then explains the techniques we use to identify close pairs and to correct for contamination by random projections. In Section 4 we calibrate the timescale which relates pair counts to merger rates. Finally the results are discussed and summarised in Section 5.

2   MODEL

2.1   The Millennium N-body simulation

We make use of the Millennium Simulation, a very large simulation which follows the hierarchical growth of dark matter structures from redshift $z = 127$ to the present. The simulation assumes

the concordance ΛCDM cosmology and follows the trajectories of $2160^3 \sim 10^{10}$ particles in a periodic box $500\,h^{-1}$Mpc on a side, using a special reduced-memory version of the GADGET-2 code (Springel et al. 2001b; Springel 2005). A full description is given by Springel et al. (2005); here we summarise the main characteristics of the simulation.

The adopted cosmological parameter values are consistent with a combined analysis of the 2dFGRS (Colless et al. 2001) and the first-year WMAP data (Spergel et al. 2003; Seljak et al. 2005). Specifically, the simulation takes $\Omega_m = \Omega_{dm} + \Omega_b = 0.25$, $\Omega_b = 0.045$, $h = 0.73$, $\Omega_\Lambda = 0.75$, $n = 1$, and $\sigma_8 = 0.9$, where all parameters are defined in the standard way. The adopted particle number and simulation volume imply a particle mass of $8.6 \times 10^8\,h^{-1}M_\odot$. This mass resolution is sufficient to represent haloes hosting galaxies as faint as $0.1\,L_\star$ with at least ~ 100 particles. The short-range gravitational force law is softened on a comoving scale of $5\,h^{-1}$kpc which may be taken as the spatial resolution limit of the calculation. The effective dynamic range is thus 10^5 in spatial scale. Data from the simulation were stored at 63 epochs spaced approximately logarithmically in time at early times and approximately linearly in time at late times (with $\Delta t \sim 300$Myr). Post-processing software identified all resolved dark haloes and their subhaloes in each of these outputs and then linked them together between neighboring outputs to construct a detailed formation tree for every halo (and its substructure) present at the final time. The formation and evolution of the galaxy population is then simulated in post-processing using this stored halo merger tree, as described in the following subsection.

2.2   The semi-analytic model

Our semi-analytic model is that of Croton et al. (2006) as updated by De Lucia & Blaizot (2007) and made public on the Millennium Simulation data download site[1]. These models include the physical processes and modelling techniques originally introduced by White & Frenk (1991); Kauffmann et al. (1993); Kauffmann & Charlot (1998); Kauffmann et al. (1999); Kauffmann & Haehnelt (2000); Springel et al. (2001a) and De Lucia et al. (2004), principally gas cooling, star formation, chemical and hydrodynamic feedback from supernovae, stellar population synthesis modelling of photometric evolution and growth of supermassive black holes by accretion and merging. They also include a treatment (based on that of Kravtsov et al. 2004) of the suppression of infall onto dwarf galaxies as consequence of reionisation heating. More importantly, they include an entirely new treatment of "radio mode" feedback from galaxies at the centres of groups and clusters containing a static hot gas atmosphere. The equations specifying the various aspects of the model and the specific parameter choices made are listed in Croton et al. (2006) and De Lucia & Blaizot (2007). The only change made here is in the dust model as described in Kitzbichler & White (2007).

We note that most of the assumptions made for the semi-analytic model only affect our merger rate study in an indirect way by influencing how merging systems are identified with observed galaxies. The dynamics of the underlying distribution of dark matter haloes and subhaloes is not changed in any way by the galaxy formation modelling. Only when the subhalo which hosts a galaxy is tidally disrupted near the centre of a more massive halo does

---

[1]   http://www.mpa-garching.mpg.de/millennium; see Lemson et al. (2006)

the galaxy become eligible to merge with the central galaxy of that halo. The merger does not occur immediately, but rather after a "dynamical friction time" estimated, following Binney & Tremaine (1987), from the relative orbit of the two objects at the moment of subhalo disruption:

$$t_{\rm fric} = 1.17 \frac{V_{\rm vir} r_{\rm sat}^2}{G m_{\rm sat} \ln \Lambda} , \qquad (1)$$

where $m_{\rm sat}$ and $r_{\rm sat}$ are the satellite subhalo mass and halo-centric distance respectively, and the Coulomb logarithm is approximated by $\ln \Lambda = \ln(1 + M_{\rm vir}/m_{\rm sat})$. This difference between the merger trees of galaxies and those of haloes (which are assumed to merge at the instant of subhalo disruption) is necessary since (sub)haloes can be identified only down to a certain mass threshold. Depending on the masses of the host and satellite subhalos, the subhalo finder typically loses track of a subhalo when tidal stripping has reduced its mass and dynamical friction has shrunk its orbit to the point where it can no longer be distinguished as a self-bound overdensity within the larger system. It is then considered to be disrupted. This typically occurs at radius $R \geqslant 1/10 \, R_{\rm vir}$, even for initially massive satellites. This is substantially greater than the separations from which the final galaxy merger is expected to occur. Thus, once the subhalo disrupts, the galaxy evolution model waits for a time $t_{\rm fric}$ before merging its associated galaxy into the central galaxy of the main halo. During this period the satellite galaxy has no associated subhalo and it is assumed to remain attached to the particle which was most strongly bound within its last identified subhalo.[2]

We can demonstrate that this treatment is required to obtain a realistic population of close pairs by comparing the two-point correlations of our simulated galaxies to those measured for real galaxies on scales $r_p < 100 \, h^{-1}$kpc. Such a test is presented in Fig. 1, which compares the projected 2-point correlation function $w_p(r_p)$ at $z = 0$ to those derived from the SDSS survey by Li et al. (2006) for five disjoint ranges of stellar mass. The solid black lines denote results from the simulation including all galaxies whereas the dotted lines exclude "orphan" galaxies that have already lost their surrounding (sub)halo and so shows the correlations expected for $t_{\rm fric} = 0$. Clearly the observations cannot be fitted on small scales by such an instantaneous merging model. The disagreement is particularly bad for low-mass galaxies, where $w_p(r_p)$ is under-predicted by at least a factor of 5 at scales below $r_p < 100 \, h^{-1}$kpc. Observed estimates of merger rates are typically based on counts of pairs at separations below 50 kpc, so it is clearly critical to include the "orphan galaxies" when calibrating the conversion from pair counts to merger rates. Note that the observable abundance of close pairs, after correction for random projections, $n_{\rm pairs}$, is straightforwardly connected to $w_p(r_p)$ through the integral

$$n_{\rm pairs}(r_l) = 2\pi n^2 \int_0^{r_l} w_p(r_p) \, r_p \, dr_p \qquad (2)$$

where n is the overall mean density of galaxies of the type included in the pair sample and r_l is the limiting projected separation for which pairs are counted.
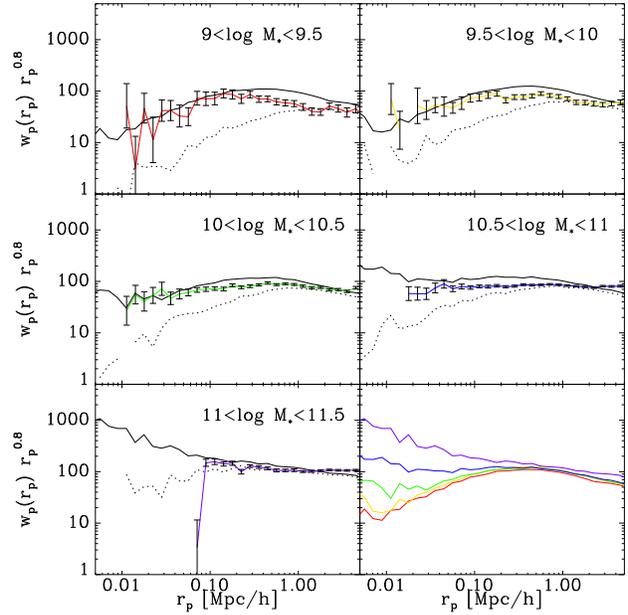
Figure 1. Projected 2-point correlation function $w_p(r_p)$ for five disjoint stellar mass ranges both including (solid) and excluding (dashed) galaxies that have lost their DM subhalo. We have multiplied $w_p(r_p)$ by $r_p^{0.8}$ in order to reduce the dynamic range of the plots and highlight differences between models and observation. In the bottom right panel the simulation results (including "orphan galaxies") for all five mass ranges are superposed. Stellar mass increases with colour from red to purple. The symbols with error bars are data from the SDSS survey taken from Li et al. (2006).

2.3 Merger rates and pair counts

Clearly a realistic treatment of galaxy merging is crucial for our study since we assume that the relation between simulated close pairs and simulated mergers is a good representation of the real relation. On the other hand, it is important to realise that the overall merger rates in the simulation reflect the hierarchical growth of dark halos as represented by the halo/subhalo merger trees built from the Millennium Simulation. This determines which galaxy pairs arrive when on the tightly bound orbits from which mergers take place. The semi-analytic treatment of the final stages merely determines how long each orphan–central galaxy pair "waits" on its tightly bound orbit before merging. For massive pairs of the kind relevant to most observational studies of merger rate evolution, these waiting times are often short compared to the age of the universe at the relevant redshifts. Thus, writing the merging rate of orphan–central pairs of any particular type as a convolution of the rate at which they are created through subhalo disruption with the distribution of merging times (eq. 1),

$$\dot{N}_{\rm merger}(t) = \int_0^\infty \dot{N}_{\rm orphan}(t - t_{\rm fric}) P(t_{\rm fric}) \, dt_{\rm fric}, \qquad (3)$$

we see that if $P(t_{\rm fric})$, the distribution of dynamical friction timescales, is confined to values smaller than the timescales on which $\dot{N}_{\rm orphan}$ varies, then $\dot{N}_{\rm merger} \approx \dot{N}_{\rm orphan}$ and the semianalytic treatment has no significant effect on the merging rate. If, on the other hand, $P(t_{\rm fric})$ has a significant tail out to and beyond the age of the universe, the two rates can differ significantly. Since subhalos can survive for a substantial time before they are tidally disrupted by their host, $\dot{N}_{\rm orphan}$ differs in a similar way from the rate at which satellite–central pairs are created through halo merg-

---

[2] Note that in the model of De Lucia & Blaizot (2007) which we are using, the coefficient in equ. 1 was multiplied by a factor of two. This brings its predictions into better agreement with the recent numerical results of Boylan-Kolchin et al. (2008).

ing. It is this latter rate which is often taken as a surrogate for the galaxy merger rate.

We illustrate these differences in Fig. 2 which focusses on pairs of galaxies with individual stellar masses differing by less than a factor of four and lying above the lower limits given as labels in each panel. The red curves show the rates at which satellite–central pairs are created by merging of their parent FOF halos. The green curves show the rate at which corresponding orphan–central galaxy pairs are created as subhalos disrupt, while the black curve shows the actual merger rate of these galaxy pairs. Clearly, the delays are significant. The orphan creation rate is a factor of two or more below the satellite creation rate at all redshifts and for all galaxy masses, while the galaxy merging rate is smaller again except near $z = 0$. The first difference shows that many new satellites retain their dark matter (sub)halos for a long time. The second shows that substantial numbers of orphan galaxies are born with relatively large $t_{\rm fric}$. Note also that while the creation rates of satellite and orphan pairs both scale approximately as $(1 + z)^{1.5}$ at low redshift, delay effects cause the low-z galaxy merger rate to be almost independent of redshift (see below).

As we already saw in Fig. 1, at projected separations of a few tens of kpc, counts of galaxy pairs in the Millennium Simulation are dominated by orphan–central pairs. Thus we can approximate the abundance of observed close pairs of any particular type as

$$N_{\rm closepair}(t) \approx \langle F\, t_{\rm fric}\rangle\, \dot{N}_{\rm orphan}(t), \qquad (4)$$

where F is a geometric factor specifying the fraction of the time a particular orphan–central pair satisfies the observational definition of a close pair when viewed from a random direction, the angle brackets specify an average over all newly created pairs of the specified type, and we assume that contributions to the average from pairs with large $t_{\rm fric}$ can be neglected. Thus we can write,

$$\dot{N}_{\rm mergers}(t) \approx T^{-1} N_{\rm closepair}(t), \qquad (5)$$

where the mean timescale T is defined by

$$T \equiv f\langle F\, t_{\rm fric}\rangle, \qquad (6)$$

with

$$f \equiv \frac{\dot{N}_{\rm orphan}}{\dot{N}_{\rm mergers}}. \qquad (7)$$

According to Figure 2, the ratio f increases from 1 to about 3 as z increases from 0 to 2. Equation 5 is the standard form used to convert close pair counts to a merger rate in observational studies. Equation 6 shows how the appropriate timescale T should be estimated in the Millennium Simulation. In practice, we obtain it directly from the simulation data by comparing the number of "observed" close pairs with the merging rate. Equation 5 also shows how the dynamical friction timescales assumed by our semi-analytic model (equation 1) are reflected in its predictions for close pair abundances. The good agreement with observation in Fig. 1 thus confirms that our assumptions are realistic. Observational studies often assume $T \sim 500$ Myr for pair samples with projected separations below $30\, h^{-1}$kpc. As we will see in Section 4.1, this is an underestimate, so the resulting merger rates are overestimates.

2.4 Merger rates for DM haloes and galaxies

Here we digress slightly to discuss further the halo and galaxy merger rates plotted in Fig. 2. It is immediately apparent that all rates peak at higher redshift for smaller objects. This is because
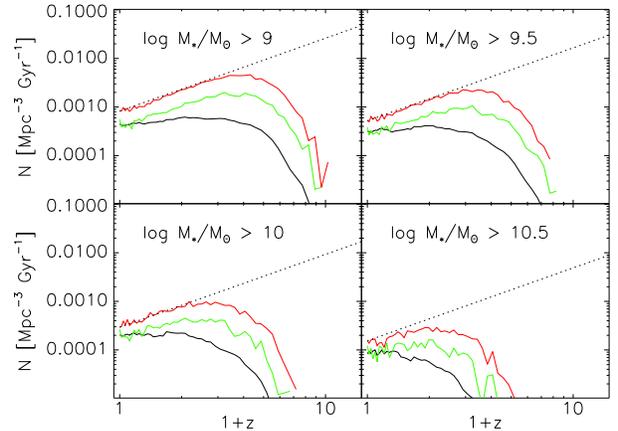

Figure 2. The variation with redshift of the rate at which halo mergers create satellite–central galaxy pairs with stellar masses differing by less than a factor of four (red lines) is compared with the rate at which such pairs are converted to orphan–central pairs by subhalo disruption (green lines) and with the rate at which such pairs merge (black lines). The four panels are for pair samples in which the stellar masses of the individual galaxies lie above the four lower limits indicated. The dotted line is a powerlaw $\dot{N} \propto (1 + z)^{1.5}$ which represents the low-redshift behaviour of the halo merging and satellite disruption rates, but does *not* fit the galaxy merger rate.

more massive objects assemble later in hierarchical models of the kind simulated here, and merger rates scale as the square of the abundance of the merging population. The analytic treatment of *halo* mergers by Lacey & Cole (1993), based on the excursion set formalism (see Press & Schechter 1974; Bond et al. 1991), shows this behaviour clearly and agrees moderately well with rates as a function of halo mass and redshift in the Millennium Simulation; however, *galaxy* merger rates in the simulation depend on stellar mass and redshift in quite a different way. For major mergers with $M_* > 10^{10}\, h^{-1}{\rm M}_\odot$ the galaxy merger rate depends strongly on stellar mass but only weakly on redshift out to $z = 1$, whereas the opposite is true for dark halos (see also Guo & White 2008).

Recent observational results for galaxy mergers by Lin et al. (2004) and Lotz et al. (2006) found a weak dependence on redshift, and these authors noted the contradiction with theoretical predictions based on DM halo merger rates. The contradiction was further explored by Berrier et al. (2006), who investigated it using HOD modelling. They inferred that the observed evolution in merger rates requires lower halo occupation numbers at higher redshift. This agrees with our more detailed semi-analytic treatment where it is a consequence of the accumulation of satellite galaxies in massive host haloes as a result their extended disruption and merging time distributions. As is obvious from Fig. 1, a realistic treatment of the accumulation requires not only the resolution of dark matter subhalos and their associated galaxies within groups and clusters, but also a proper treatment of orphan galaxies after their associated subhalo is disrupted.

Berrier et al. (2006) conclude that measuring galaxy merger rates is an important tool to understand the formation and evolution of galaxies, but is a poor probe of the cosmological aspects of structure formation; the connection to theoretically predicted halo merger rates is subject to too many uncertainties. The discrepancies seen in Fig. 2 support this view. On the other hand, with the advent of the *concordance cosmology* most cosmological parameters appear well determined, and exploring the details of galaxy formation is perhaps a more urgent cause. The calibration of the galaxy

merging timescale presented below accounts realistically for differences between halo and galaxy behaviour, as judged by the fact that the Millennium Simulation reproduces the observed clustering of galaxies down to small scales. Nevertheless, further improvements of several aspects of our modelling of the underlying physical processes are needed before our calibration can be considered definitive.

2.5 The mock lightcone

The fundamental question we are addressing in this paper is how well the merger rate of galaxies can be recovered as a function of galaxy properties from the abundance of close pairs of galaxies on the sky. The most direct way to assess this is to create "mock catalogues" from our simulation which correspond as closely as possible to real survey catalogues, and then to mimic observational procedures. To this end we place a virtual observer at the origin of our simulation box and calculate which galaxies fall onto his backward lightcone [3]. For the nearby universe these galaxies will lie in the $z = 0$ snapshot of the simulation, but as we go out along the line-of-sight we must populate the field-of-view with galaxies from progressively earlier snapshots. We must also interpolate redshifts, and most importantly luminosities through various observer-frame filters, between snapshots in order to get the appropriate values for "observed" properties. A more detailed account of the methods we use to produce mock observations from the Millennium Run semi-analytic galaxy catalogues may be found in Kitzbichler & White (2007).

For the study presented in this paper we chose a field of view of $10 \times 1.4 \deg^2$ which we found to be a good compromise between ensuring a sufficiently large sample for robust statistics at all redshifts of interest and maintaining computational efficiency. We adopt a limiting apparent magnitude of $B_{AB} \leqslant 26$, close to the current effective limit for photometric surveys of moderately large areas, and well beyond the current limit for reliable multi-object spectroscopy. Note that because of the limited resolution of the Millennium Simulation, our model galaxy catalogues become incomplete at absolute magnitudes fainter than about $M_B < -16$, and as a result our lightcone will miss intrinsically faint galaxies at all but the highest redshifts. This will not affect our later analysis which is restricted to bright and massive systems.

Our final mock catalogue contains 3236337 galaxies. In Fig. 3 we depict their spatial distribution out to $z = 1$ in order to illustrate the structure in this mock lightcone. The filaments and voids emerge vividly in this plot, where we encode projected galaxy density as intensity and satellite galaxy fraction as colour. Clearly many galaxies in the most clustered regions are satellites, whereas in the filaments and the sparsely populated regions, most galaxies are the central systems of their halos.

[3] The backward lightcone is defined as the set of all light-like worldlines intersecting the position of the observer at redshift zero. It is thus a three-dimensional hypersurface in four-dimensional space-time satisfying the condition that light emitted from every point is received by the observer now. Its space-like projection is the volume within the observer's current particle horizon.

3 PAIR SELECTION METHODS

3.1 Finding pairs

A limitation of our mocks in comparison to real catalogues is that they include no record of recent close interactions which might be related to the morphological indicators accessible with high-quality deep imaging. Many authors, beginning with Toomre & Toomre (1972) and Larson & Tinsley (1978) have shown that close encounters between massive galaxies can produce both enhanced star formation and disturbed morphologies (e.g Patton et al. 2005; Lin et al. 2006; Li et al. 2008, and references therein). Detection of such effects is a clear indicator that apparent proximity on the sky does indeed correspond to physical interaction, and so greatly increases the level of confidence that a given close pair is likely to merge. On the other hand, the detectability of these effects depends strongly on the quality of the imaging, on the structure of the merging galaxies, and on the time, viewing angle and redshift at which they are observed. As a result it is very difficult to estimate what fraction of close pre-merger pairs will be detected by any given set of morphological criteria. This makes it impossible to estimate merger rates reliably from such samples.

Until recently, observational studies of merging typically involved from a few dozen to a few hundred pairs. Every pair could be examined visually to assess whether it is interacting. Current and future surveys will produce much larger samples for analysis, necessitating automatic techniques to search for morphological signatures of interaction. The reliability of such classification techniques depends crucially on good signal-to-noise and adequate resolution. When these conditions are met, measures of concentration, asymmetry and clumpiness can be combined with other indices such as the *Gini* and M_{20} coefficients of Lotz et al. (2004) to produce very large samples of galaxies with a morphological classification (see e.g. Abraham et al. 2003; Prescott et al. 2004; Zamojski et al. 2006), of which $1 - 3\%$ typically show signatures of an ongoing interaction. For the reasons noted above, however, such samples are not suitable for estimating merger rates. For the rest of this paper we will therefore concentrate on pair samples selected purely by the proximity of the two galaxies.

3.1.1 Pair samples from imaging alone

The most straightforward way to find pairs of galaxies is simply to identify objects which are close together on the sky in a purely photometric survey. This technique was used for some of the earliest pair fraction studies (e.g. Zepf & Koo 1989) because it could be applied to any survey with a large enough galaxy catalogue (> 1000 at that time). One must keep in mind that the close pair fraction is of order a few percent, so to get acceptable statistics for the pair sample, the original catalogue must be much larger. The disadvantage of this purely photometric method is, of course, that one will inadvertently include many false pairs, i.e. chance projections that are not physically close. This "background noise" becomes more problematic for higher mean galaxy densities on the sky, corresponding to deeper magnitude limits; early studies worked moderately well *because* of their shallow limits.

The fraction F of true companions in a sample of apparent pairs can be estimated from the angular correlation function $w(\theta)$ as $F = w/(1+w)$. Only for $w(\theta) > 1$ are the majority of apparent companions at angular distance θ true physical companions. According to Limber's equation (Limber 1953) the angular two-point correlation function depends on limiting flux density $f = {}^L/4\pi r^2$ as
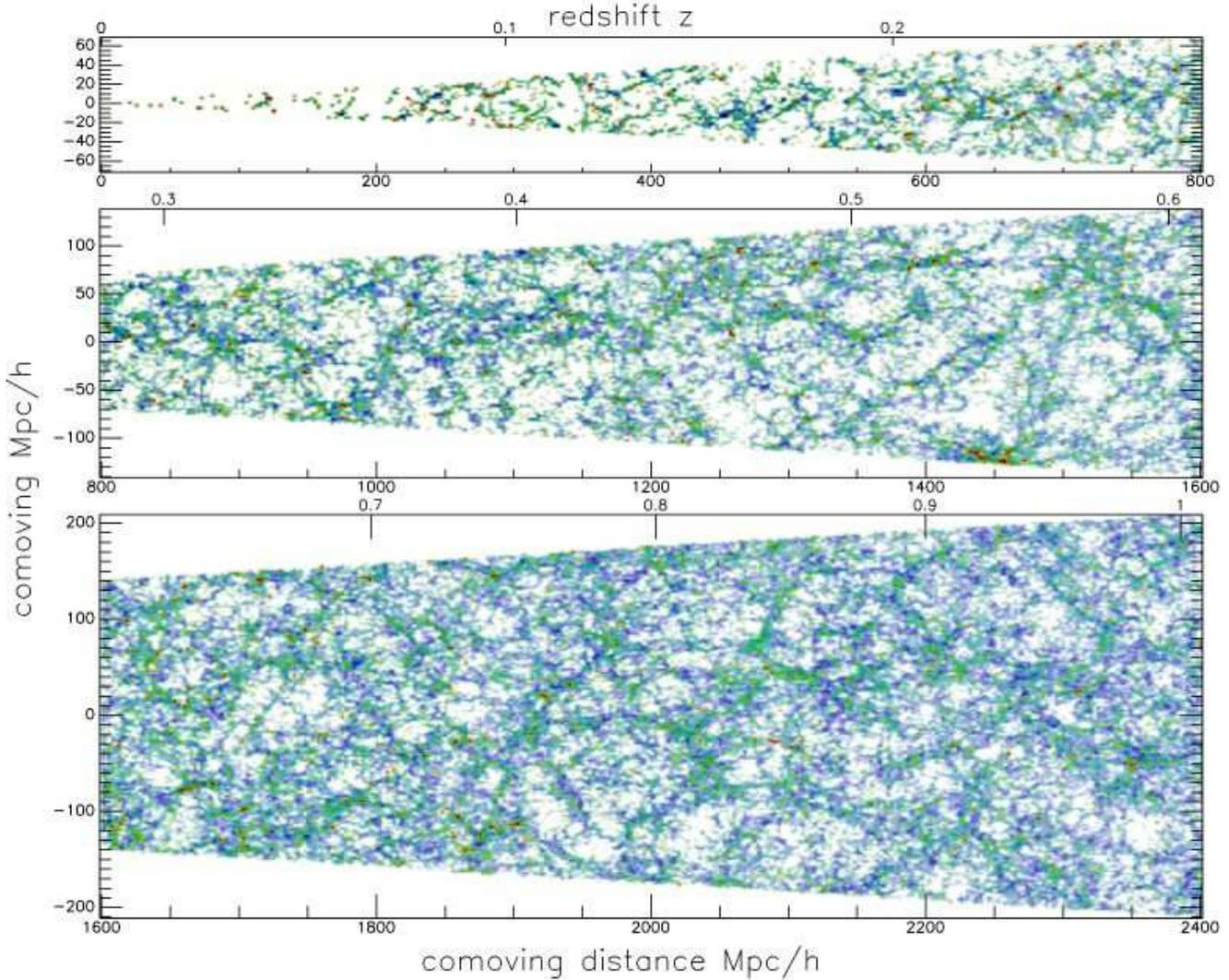
Figure 3. A lightcone with a field of view of $10 \times 1.4 \deg^2$ which we use for close pair and merger rate studies. The colour map encodes projected galaxy density as intensity and satellite galaxy fraction as colour (from blue to red). Only the region out to $z = 1$ is displayed, although the cone actually extends to $z \sim 5$.

$w(\theta) \propto f^{\gamma/2}$ (assuming a power law $\xi = (r_0/r)^\gamma$ for the spatial function with r_0 independent of distance). For surveys as deep as we simulate here, $w(\theta) \sim 1$ corresponds to $\theta \sim 0.1$arcsec so that observationally realistic samples of close pairs (typically limited to separations of a few arcseconds) are entirely dominated by chance projections. Although for large samples the fraction of "true" close pairs can be determined statistically with high reliability, it is impossible to know *which* close pairs are interacting without additional information, for example from morphologies. Furthermore, without spectroscopy the separation distribution (in 3-D) of the true pairs and its dependence on redshift cannot be derived from the observed angular separation distribution without making additional assumptions about the redshift distribution of the population and the evolution of its clustering.

3.1.2 Primary redshift catalogue with photometric companions

Many recent pair studies (e.g. Yee & Ellingson 1995) have been based on correlating a redshift survey with a deeper photometric catalogue. This allows the identification of all close apparent

companions for a complete set of galaxies of known distance and brightness. For sufficiently large samples the projected correlation function $w_p(r_p, z)$ can be estimated, giving the abundance of true physical pairs as a function of projected separation r_p. Assuming isotropy of orientation for the underlying population, this can be inverted to give the distribution of companions as a function of 3-D separation, and thus the abundance of companions within some maximal separation (e.g. 30 kpc). Note that without morphological information one still has no indication of *which* apparent pairs are actually physically close. This problem is significant in deep surveys where the majority of apparent projections are chance superpositions of unrelated objects. The major advantage of starting with a redshift survey is that the dependences of the close pair distribution on physical separation and on redshift can be determined separately.

3.1.3 Photometric redshift pair identification

If photometric redshifts are available for all galaxies in a catalogue, this allows the definition of still purer samples of physical pairs.

Here also one can define a physical (rather than angular) search radius around each galaxy, and additionally one can limit acceptable pairs to those whose redshifts are equal to within the accuracy of the photometric determinations. Some correction for random pairs is still required, however, since this accuracy is sufficiently poor that projected pairs with moderately large true redshift differences can still enter the sample. The number of "true" pairs at any given apparent separation r_p and redshift z within some photometric redshift tolerance Δz can be found by taking the number of such pairs counted in the real catalogue and subtracting the mean number found in a large number of artificial catalogues in which the photometric redshifts of the galaxies are retained but their angular positions within the survey area are randomised.

3.1.4 Complete spectroscopic redshift samples

Clearly the ideal sample for a pair study is one that includes accurate spectroscopic redshifts for all galaxies. This allows a search for "true" physical companions in the space of projected physical separation and velocity difference. The result is an unbiased sample with minimal contamination by optical pairs. In principle, a correction for random pairs can be applied just as in the previous section, but in practice this correction is so small that it can be neglected. Additionally, one can estimate the fraction of the physical pair population which corresponds to truly close pairs, i.e. to pairs for which the 3-D separation is also small.

3.2 Identifying candidate pairs for mergers

From our mock survey lightcone we construct several close pair samples as follows. For each galaxy we examine the 20 closest companions on the sky and apply various criteria to define pair subsets that we consider as merger candidates. These criteria include: (i) projected physical separation r_p, (ii) radial velocity difference Δv, (iii) redshift difference Δz. We apply these cuts in different combinations to build different samples. In addition, we distinguish pairs by the stellar mass ratio of the two pair members.

For the rest of this paper we will concentrate on potential major mergers which we define to be pairs with stellar mass ratios of 4:1 or less. This restriction is applied for several reasons. First, observational studies usually concentrate on galaxy pairs with small magnitude differences, either because both galaxies are typically close to the apparent magnitude limit of the parent survey, or because a limit on apparent magnitude difference is applied explicitly. This is to prevent confusion between actual companions and morphological features in the outer regions of a bright galaxy. Restricting galaxy pairs to a narrow range of mass ratios also makes sense from a theoretical point of view, since it is the growth of galaxies through major mergers that dominates the morphological transformation of galaxies.

Using the criteria listed above we define a number of samples. For the projected physical (i.e. *not* comoving) distance r_p we choose maximal values of 30, 50, or 100 h^{-1}kpc. To mimic "spectroscopic" samples, we assume infinitely accurate redshifts and select pairs with radial velocity differences $\Delta v < 300\,\mathrm{km\,s^{-1}}$. (Note that this excludes a number of true physical pairs with larger velocity separation, but most such pairs are within massive clusters and so rarely merge.) For "photo-z" samples we require a redshift difference of $\Delta z < 0.05$. In the following sections we will use pair samples defined in this way to study the relation between close pairs of galaxies and mergers.
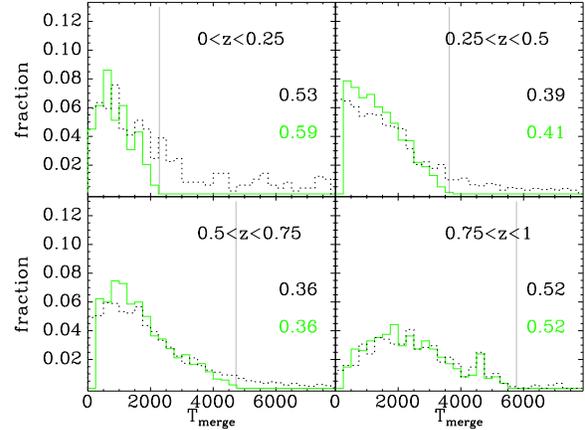

Figure 4. Distribution of merging times for galaxies more massive than $M_* > 10^{10}\,h^{-1}\mathrm{M}_\odot$ at four different redshifts. Pairs are selected from the lightcone with $r_p < 50\,h^{-1}$kpc and $\Delta v < 300\,\mathrm{km\,s^{-1}}$. For the green histograms, merging times were determined by following the galaxies forward in time until they merge (or reach $z = 0$). The timespan between the highest redshift contributing to each panel and $z = 0$ is indicated by the grey vertical line. For the black histograms, merging times were determined using the internal counters set when one of the galaxies first loses its dark halo. (This can occur before or after the pair is actually identified in the lightcone.) All samples are subject to an apparent magnitude cut at $B < 26$ and only major mergers are considered. The coloured numbers in each panel give the fraction of all pairs which are not predicted to merge by $z = 0$.
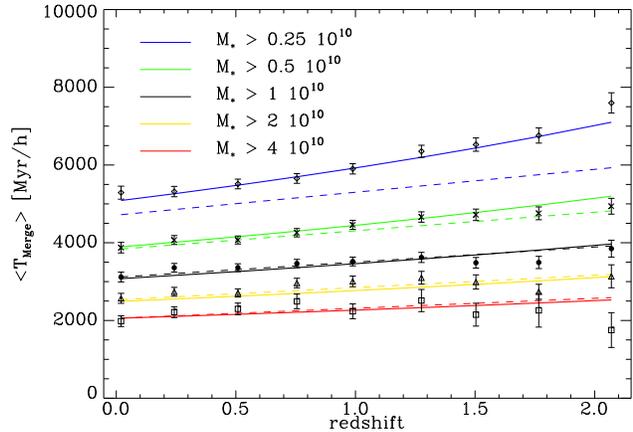

Figure 5. Redshift evolution of the timescale $T = N_{\mathrm{pairs}}/\dot{N}_{\mathrm{Merge}}$ for conversion from pair fraction to merger rate. Two-dimensional linear regression fits (Eqn. 9) are plotted as solid curves for a range of mass cuts denoted by different colours, as indicated by the labels. The corresponding data are indicated by points with error bars. All pair samples in this plot were selected requiring projected separations $r_p < 50\,h^{-1}$kpc, radial velocity difference s$\Delta v < 300\,\mathrm{km\,s^{-1}}$, and galaxy stellar masses differing by a factor less than 4. The dashed lines are for the simplified fitting function of Eqn. 10.

4 RESULTS

4.1 Distribution of merging times

In Fig. 4 we show distributions of merging times for close pairs of galaxies in our lightcone with $r_p < 50\,h^{-1}$kpc, $\Delta v < 300\,\mathrm{km\,s^{-1}}$, individual apparent magnitudes $B < 26$, and individual stellar

masses which exceed $10^{10} \, h^{-1} \mathrm{M}_\odot$ and differ by less than a factor of 4. The four panels show distributions for four disjoint redshift ranges as indicated. Merging times were determined either by following the later evolution of each pair until merging (or until $z = 0$; the green histograms) or by using the time-until-merger counter assigned to each orphan galaxy at the time it is orphaned (the dashed black histogram). The distributions are plotted as the fraction of *all* pairs in each histogram bin, and so do not normalise to unity in the green case. The fraction of pairs which do *not* merge by $z = 0$ is indicated in each panel by labels of the appropriate colour.

The most important results to note from this figure are that the merger time distributions vary little with redshift, that they extend to large values, and that they include the majority of pairs. Most close pairs eventually merge, even for $r_p < 50 \, h^{-1} \mathrm{kpc}$. These results are best seen from the black histograms. These indicate a median merger time above 2 Gyr, much longer than the merging times typically adopted when estimating merger rates from observed pair counts. At lower redshifts, the directly estimated merger-time distributions do not extend to large times. This simply reflects the fact that there is insufficient time for many of the mergers to take place, as may be seen from the vertical grey lines which give the lookback time to the largest redshift used when constructing the distributions in each panel. The black histograms show how much longer one would have to wait for the other objects to merge. At mergertimes below this limit there is good agreement between the directly and indirectly estimated distributions (the black and the green histograms).

The distributions of merger-times in the highest redshift panel appear to have fewer pairs with short merger times than those at lower redshift. This is because the imposed apparent magnitude limit at $B > 26$ excludes significant numbers of galaxies from the sample at these redshifts. The galaxies that are lost are primarily red systems close to our mass cut at $10^{10} \, h^{-1} \mathrm{M}_\odot$. These are almost all satellite systems which have had substantial time to age and dim since their accretion; they are thus typically "about" to merge. This effect is also responsible for the fact that the fraction of observed pairs which do *not* merge by $z = 0$ increases in the highest redshift panel, reversing the trend in the other panels. It seems that selection effects may, in some circumstances, bias observational samples against pre-merger pairs, although interaction-induced star formation (which is not included in our galaxy modelling) could well reduce or even reverse this bias.

4.2 Mean merging times

We have established that, for the separation and velocity difference cuts typically adopted, most close pairs of similar mass galaxies will, in fact, merge. We can therefore address the main issue of this paper, namely: "What timescale should be used to convert counts of such close pairs into a merger rate?" As noted in Eqn. 5, this timescale is simply the ratio at each redshift of the abundance of pairs of a particular type to the merger rate of such pairs per unit volume,

$$\langle T_{\mathrm{merge}} \rangle = N_{\mathrm{pairs}} / \dot{N}_{\mathrm{merge}}. \tag{8}$$

Calculating this ratio as a function of redshift and mass cut for pairs with $r_p < 50 \, h^{-1} \mathrm{kpc}$ and $\Delta v < 300 \, \mathrm{km \, s^{-1}}$ yields the results presented in Fig. 5. Since the square root of the inverse of this dependency seems to be linear within the scatter for mass cuts below $10^{10} \, h^{-1} \mathrm{M}_\odot$, we decided to apply a two-dimensional linear regression to $\langle T_{\mathrm{merge}} \rangle^{-1/2} \equiv T^{-1/2}(z, M_*)$ as a function of z and $\log M_*$, implying the relation

$$\langle T_{\mathrm{merge}} \rangle^{-1/2} = T_0^{-1/2} + f_1 \, z + f_2 \, (\log M_* - 10) \, . \tag{9}$$

The value of T_0 as well as the coefficients f_x and their uncertainties estimated from fits to all our numerical data are tabulated for samples with different pair identification criteria in Table 1.

In the low redshift regime ($z \leqslant 1$) and for stellar masses above $5 \times 10^9 \, h^{-1} \mathrm{M}_\odot$ an even simpler fitting formula works well:

$$\langle T_{\mathrm{merge}} \rangle = 2.2 \mathrm{Gyr} \frac{r_p}{50 \mathrm{kpc}} \left(\frac{M_*}{4 \cdot 10^{10} \, h^{-1} \mathrm{M}_\odot} \right)^{-0.3} (1 + \frac{z}{8}) \tag{10}$$

for samples restricted to $\Delta v < 300 \, \mathrm{km \, s^{-1}}$ and

$$\langle T_{\mathrm{merge}} \rangle = 3.2 \mathrm{Gyr} \frac{r_p}{50 \mathrm{kpc}} \left(\frac{M_*}{4 \cdot 10^{10} \, h^{-1} \mathrm{M}_\odot} \right)^{-0.3} (1 + \frac{z}{20}) \tag{11}$$

for samples limited to $\Delta v < 3000 \, \mathrm{km \, s^{-1}}$. These simplified fits give the results indicated by the dashed lines in Fig. 5. The difference in the normalisation coefficient between the two cases reflects the fact that expanding the velocity cut admits about 50% more pairs. Most of these additional pairs are physically associated but lie within larger groups or clusters. The timescales for $\Delta v < 3000 \, \mathrm{km \, s^{-1}}$ should be used when analysing data from photometric redshift samples, since the "background" correction will not eliminate physically associated galaxies at large velocity separation.

Aside from the dependence on mass cut and redshift that is illustrated in this figure, there is also a strong dependence on the maximum projected radius r_p. This is a natural consequence of Eqn. 8, since the denominator $\dot{N}_{\mathrm{merge}}$ is independent of r_p whereas the numerator N_{pairs} is not. The latter is proportional to the integral of the projected 2-point correlation function $w_p(r)$ out to r_p (see Eqn. 2). If we choose the usual parametrisation $w_p \sim (r/r_0)^{-\alpha}$ we get $N_{\mathrm{pairs}} \sim r_p^{2-\alpha}$, where $\alpha = 0.8$ is commonly adopted in the literature. Thus we would expect the values in the table to scale as $r_p^{1.2}$ which is qualitatively consistent with the actual values but slightly too strong. If we instead calculate α from the measured values, we get $\alpha = 1.06$ and $\alpha = 0.93$ for the intervals 30-50 $h^{-1} \mathrm{kpc}$ and 50-100 $h^{-1} \mathrm{kpc}$ respectively. This is consistent with Fig. 1 where we see that the projected 2-point correlation function on scales below $100 \, h^{-1} \mathrm{kpc}$ and for masses above $3 \cdot 10^{10} \, h^{-1} \mathrm{M}_\odot$ is considerably steeper than the fiducial $\alpha = 0.8$.

The mean merging times found here are clearly consistent with the distribution of individual merging times shown in Fig. 4. They are also much larger than the values ~ 0.5 Gyr typically adopted in observational studies of this problem. As a result most earlier studies have substantially overestimated merger rates.

5 CONCLUSIONS

We have investigated major merger rates in our semi-analytic model based on the Millennium N-body simulation and compared them to the abundance of close galaxy pairs. In this way we have calibrated the relation used to estimate merger rates from deep galaxy surveys. In addition, we have shown that for the parameters typically adopted in observational studies, most close pairs do indeed merge, albeit on a substantially longer timescale than is usually assumed. As a result, the characteristic timescales we derive are indeed the typical times until pair members merge. The ideal parent catalogue for such studies would contain spectroscopic redshifts for all galaxies, but in practice reliable results can be obtained from any deep photometric catalogue, provided good photometric

Table 1. Coefficients for different pair identification criteria obtained from fits of $\langle T_{\mathrm{merge}} \rangle = T(z, M_*)$ to our numerical data on $N_{\mathrm{pairs}}/\dot{N}_{\mathrm{merge}}$ according to Eqn. 9.

VELOCITY	PROJECTED DISTANCE		
$v_p < 300\,\mathrm{km\,s^{-1}}$	r_p $\leqslant 30\,\mathrm{kpc}/h$	$\leqslant 50\,\mathrm{kpc}/h$	$\leqslant 100\,\mathrm{kpc}/h$
$T_0\,[\,h^{-1}\mathrm{Myr}]$	2038	3310	6909
$10^5 f_1\,[\,h^{-1}\mathrm{Myr}^{-1/2}]$	$-165.\pm 4.4$	$-105.\pm 3.3$	-30.4 ± 2.2
$10^5 f_2\,[\,h^{-1}\mathrm{Myr}^{-1/2}]$	$690.\pm 10.$	$668.\pm 7.7$	$571.\pm 5.2$
$v_p < 3000\,\mathrm{km\,s^{-1}}$	r_p $\leqslant 30\,\mathrm{kpc}/h$	$\leqslant 50\,\mathrm{kpc}/h$	$\leqslant 100\,\mathrm{kpc}/h$
$T_0\,[\,h^{-1}\mathrm{Myr}]$	2806	4971	11412
$10^5 f_1\,[\,h^{-1}\mathrm{Myr}^{-1/2}]$	-94.7 ± 3.7	-38.6 ± 2.7	18.0 ± 1.7
$10^5 f_2\,[\,h^{-1}\mathrm{Myr}^{-1/2}]$	$671.\pm 8.7$	$615.\pm 6.3$	$491.\pm 4.2$

redshifts are available and care is taken to correct for chance line-of-sight projections. The main advantage of using photo-z's is, of course, that they allow results to be obtained for much larger and deeper samples than could otherwise be used. Their main disadvantage is that one does not know which close pairs are "physical" and which are random projections.

The main results of our study are as follows:

(i) The characteristic timescale which converts background-corrected pair counts into merger rates (Fig. 5) depends on the pair identification criteria, on the stellar mass cut and weakly on the redshift. For stellar masses above $5 \times 10^9\,h^{-1}\mathrm{M}_\odot$ it can be approximated by the simple relations

$$\langle T_{\mathrm{merge}} \rangle = 2.2\mathrm{Gyr}\frac{r_p}{50\mathrm{kpc}}\left(\frac{M_*}{4 \cdot 10^{10}\,h^{-1}\mathrm{M}_\odot}\right)^{-0.3}\left(1+\frac{z}{8}\right)$$

for radial velocity differences $\Delta v < 300\,\mathrm{km\,s^{-1}}$ and by

$$\langle T_{\mathrm{merge}} \rangle = 3.2\mathrm{Gyr}\frac{r_p}{50\mathrm{kpc}}\left(\frac{M_*}{4 \cdot 10^{10}\,h^{-1}\mathrm{M}_\odot}\right)^{-0.3}\left(1+\frac{z}{20}\right)$$

for $\Delta v < 3000\,\mathrm{km\,s^{-1}}$. This latter relation should be used for pair counts derived from photometric redshift surveys. A more accurate fitting formula is given in Eqn. 9; the corresponding coefficients T_0, f_1 and f_2 are listed in Table 1 for a range of pair selection criteria.

(ii) The characteristic timescales we find are larger (typically by a factor of at least 2) than is assumed in most published determinations of merger rates. These are therefore likely to be substantial overestimates of the true rates.

(iii) For masses $M_* > 3 \times 10^9\,h^{-1}\mathrm{M}_\odot$, the intrinsic galaxy merger rate evolution is quite flat at low redshift, $\dot{N} \sim (1+z)^\alpha$, with $\alpha < 0.5$ and decreasing towards higher mass. For large masses the exponent becomes negative. Overall, the distributions are quite flat out to redshift $z \sim 2$ (see e.g. Fig. 2). Observational results lie in the range $N_{\mathrm{pair}} \sim (1+z)^{2\pm 2}$ where the large uncertainties are presumably due to small sample sizes and uncontrolled selection effects. In particular, effects due to the apparent magnitude limits of real surveys interact with the stellar populations of galaxies in ways which make it very difficult to define physically equivalent samples at different redshifts. We have presented most of our results for volume-limited samples in order to avoid confusion due to these complexities.

(iv) The broad distribution of merging times, peaking well beyond 1 Gyr, results in merger rates for galaxies which evolve differently from those of dark matter halos, even of halos similar in mass to those that host galaxies. At low redshifts merger rates for DM halos scale as $\dot{N} \sim (1+z)^{3/2}$ for all masses, a much more rapid evolution than we find for galaxies (Fig. 2). This discrepancy has already been described by other authors, and we agree with their conclusion that merger rate studies are less suitable for probing the overall growth of cosmic structure than originally thought. They can instead contribute substantially to our understanding of the formation and evolution of galaxies.

REFERENCES

Abraham, R. G., van den Bergh, S., & Nair, P. 2003, ApJ, 588, 218

Bell, E. F., Phleps, S., Somerville, R. S., et al. 2006, ApJ, 652, 270

Berrier, J. C., Bullock, J. S., Barton, E. J., et al. 2006, ApJ, 652, 56

Binney, J. & Tremaine, S. 1987, Galactic dynamics (Princeton, NJ, Princeton University Press, 1987, 747 p.)

Bond, J. R., Cole, S., Efstathiou, G., & Kaiser, N. 1991, ApJ, 379, 440

Boylan-Kolchin, M., Ma, C.-P., & Quataert, E. 2008, MNRAS, 383, 93

Burkey, J. M., Keel, W. C., Windhorst, R. A., & Franklin, B. E. 1994, ApJL, 429, L13

Colless, M., Dalton, G., Maddox, S., et al. 2001, MNRAS, 328, 1039

Croton, D. J., Springel, V., White, S. D. M., et al. 2006, MNRAS, 365, 11

De Lucia, G. & Blaizot, J. 2007, MNRAS, 375, 2

De Lucia, G., Kauffmann, G., & White, S. D. M. 2004, MNRAS, 349, 1101

Fall, S. M. 1979, Nature, 281, 200

Guo, Q. & White, S. D. M. 2008, MNRAS, 384, 2

Holmberg, E. 1937, Annals of the Observatory of Lund, 6, 1

Kauffmann, G. & Charlot, S. 1998, MNRAS, 294, 705

Kauffmann, G., Colberg, J. M., Diaferio, A., & White, S. D. M. 1999, MNRAS, 303, 188

Kauffmann, G. & Haehnelt, M. 2000, MNRAS, 311, 576

Kauffmann, G., White, S. D. M., & Guiderdoni, B. 1993, MNRAS, 264, 201

Khochfar, S. & Burkert, A. 2001, ApJ, 561, 517

Kitzbichler, M. G. & White, S. D. M. 2007, MNRAS, 376, 2

Kravtsov, A. V., Gnedin, O. Y., & Klypin, A. A. 2004, ApJ, 609, 482

Lacey, C. & Cole, S. 1993, MNRAS, 262, 627

Larson, R. B. & Tinsley, B. M. 1978, ApJ, 219, 46

Le Fèvre, O., Abraham, R., Lilly, S. J., et al. 2000, MNRAS, 311, 565

Lemson, G. et al. 2006, ArXiv Astrophysics: astro-ph/0608019

Li, C., Kauffmann, G., Heckman, T. M., Jing, Y. P., & White, S. D. M. 2008, MNRAS, 389

Li, C., Kauffmann, G., Jing, Y. P., et al. 2006, MNRAS, 368, 21

Limber, D. N. 1953, ApJ, 117, 134

Lin, L., Koo, D. C., Weiner, B. J., et al. 2006, ArXiv Astrophysics e-prints

Lin, L., Koo, D. C., Willmer, C. N. A., et al. 2004, ApJL, 617, L9

Lotz, J. M., Davis, M., Faber, S. M., et al. 2006, ArXiv Astrophysics e-prints

Lotz, J. M., Primack, J., & Madau, P. 2004, AJ, 128, 163

Page, T. 1952, ApJ, 116, 63

Patton, D. R., Grant, J. K., Simard, L., et al. 2005, AJ, 130, 2043

Patton, D. R., Pritchet, C. J., Yee, H. K. C., Ellingson, E., & Carlberg, R. G. 1997, ApJ, 475, 29

Prescott, M., Impey, C., Scoville, N., & COSMOS Collaboration. 2004, in Bulletin of the American Astronomical Society, Vol. 36, 728–+

Press, W. H. & Schechter, P. 1974, ApJ, 187, 425

Seljak, U., Makarov, A., McDonald, P., et al. 2005, Physical Review, 71, 103515

Spergel, D. N., Verde, L., Peiris, H. V., et al. 2003, ApJS, 148, 175

Springel, V. 2005, MNRAS, 364, 1105

Springel, V., White, S. D. M., Jenkins, A., et al. 2005, Nature, 435, 629

Springel, V., White, S. D. M., Tormen, G., & Kauffmann, G. 2001a, MNRAS, 328, 726

Springel, V., Yoshida, N., & White, S. D. M. 2001b, New Astronomy, 6, 79

Toomre, A. & Toomre, J. 1972, ApJ, 178, 623

White, S. D. M. & Frenk, C. S. 1991, ApJ, 379, 52

Woods, D., Fahlman, G. G., & Richer, H. B. 1995, ApJ, 454, 32

Yee, H. K. C. & Ellingson, E. 1995, ApJ, 445, 37

Zamojski, M. A., Schiminovich, D., Rich, M., et al. 2006, in American Astronomical Society Meeting Abstracts, Vol. 209, 225.04–+

Zepf, S. E. & Koo, D. C. 1989, ApJ, 337, 34